

Generating synthetic ultrasonic testing datasets to advance data-driven porosity detection in fibre-reinforced composites

Daniel J. Peppé

Summary

This dissertation investigates the application of machine learning (ML) to porosity detection in fibre-reinforced composites (FRCs) using synthetic ultrasonic testing (UT) datasets. A 2D finite element (FE) simulation written in MATLAB is used to generate large UT datasets for a carbon-fibre reinforced polymer (CFRP) specimen. Porosity is modelled in the specimen by reproducing the effect of porosity on the ultrasonic response rather than modelling pore size and morphology directly. ML models are trained using an automated ML (AutoML) library, AutoGluon. It is shown that the ML models can achieve up to 99% accuracy in detecting porosity within an error tolerance of $\pm 0.5\%$ porosity when tested on synthetic data, meeting the standard of some existing porosity detection techniques. Although initial results suggest the ML models perform well on real-world data, further testing is required to confirm this performance. Further investigation is recommended to test the models against a broader range of real-world data and different porosity conditions, including varying pore sizes and morphology. Recommendations are made for improving the 2D FE simulation used to generate the UT datasets. Finally, a simple framework for how the detection method could be implemented into an industrial setting is proposed.

Supervised by Professor P. Wilcox

Department of Mechanical Engineering
University of Bristol
2024

Declaration

This project report is submitted towards an application for a degree in Mechanical Engineering at the University of Bristol. The report is based upon independent work by the candidate. All contributions from others have been acknowledged and the supervisor is identified on the front page. The views expressed within the report are those of the author and not of the University of Bristol.

I hereby assert my right to be identified as the author of this report. I give permission to the University of Bristol Library to add this report to its stock and to make it available for consultation in the library, and for inter-library lending for use in another library. It may be copied in full or in part for any bona fide library or research worker on the understanding that users are made aware of their obligations under copyright legislation.

I hereby declare that the above statements are true.

A handwritten signature in black ink, appearing to read "Daniel J. Peppé".

© Copyright, Daniel J. Peppé, 2024

Certification of ownership of the copyright in a dissertation presented as part of and in accordance with the requirements for a degree in Mechanical Engineering at the University of Bristol.

This report is the property of the University of Bristol Library and may only be used with due regard to the author. Bibliographical references may be noted but no part may be copied for use or quotation in any published work without prior permission of the author. In addition, due acknowledgement for any use must be made.

Contents

1	Introduction	4
2	Ultrasonic testing background	5
3	Finite element simulation	5
3.1	Dataset requirements and scope	5
3.2	Meshing and solver specification	6
3.3	Model description	6
3.4	Model validation	9
3.5	Porosity modelling	10
4	Data generation method	12
5	Machine learning model training and testing	13
6	Results	14
7	Discussion	15
8	Conclusions & Recommendations	17

1. Introduction

The use of fibre-reinforced composites (FRCs) has grown rapidly across multiple industries in recent decades. Aerospace has particularly benefited from the development of FRCs due to their desirable material properties and high strength/stiffness-to-weight ratios [1]. Aerospace applications are often advanced, safety-critical applications which require composites to be manufactured to high quality standards to ensure the performance of the material does not deviate significantly from its designed specifications. These deviations are usually due to defects originating at the manufacturing process of the composite.

One of the most significant defects present in FRCs is voidage/porosity. This refers to sub-millimetre air pockets formed within the polymer matrix of the FRC. Both terms are used interchangeably across the literature. In this study, the term porosity is used to describe the presence of pores in FRCs. Porosity is measured as a volume fraction relative to the volume of the whole composite, so 1% porosity corresponds to a composite with 1% of its total volume being air.

Porosity is one of the most studied FRC defects due to its considerable effect on a wide range of composite properties and its high likelihood of formation from various composite manufacturing techniques [2]. Furthermore, Judd and Wright investigated the effect of porosity on the mechanical properties of FRCs and found that a 1% increase in porosity correlates with a ~6% reduction in interlaminar shear strength (ILSS) up to 4% porosity [3]. For most industry applications, 2% porosity is considered a nominal acceptance threshold [4]. Therefore, the ability to detect and measure low levels of porosity in FRCs is of great importance in ensuring the performance and reliability of parts using FRCs.

The detection of porosity can be split into destructive and non-destructive methods. Examples of destructive methods include microscopy [5], and density determination by acid digestion or ignition [6]. Examples of non-destructive methods include radiography [7], thermography [8], micro-CT (limited to small specimen sizes) [9], and ultrasonic testing (UT) [6]. The accuracy of UT varies depending on the inspection setup and the signal processing used, one study cites an accuracy of $\pm 0.5\%$ absolute porosity [10]. Density

determination is found to have a similar accuracy [6]. Each detection method has benefits and drawbacks, in general, no detection method is suitable in all cases and the best detection method depends on the needs of the specimen and inspection requirements. However, improvements in non-destructive testing methods, such as UT, offer a high value proposition for aerospace applications due to the low tolerance for porosity in FRCs, and the ubiquity of UT.

UT is one of the most widely used non-destructive methods for porosity detection [2]. This can be done by analysing the phase velocity which measures the velocity of frequency components relative to the wave packet, or by measuring the attenuation (energy loss) of a response. However, it is more common to measure attenuation because it is simpler and phase velocity is dependent on fibre-volume fraction [11]. Despite its widespread use, UT is limited by its inability to determine pore morphology, size, and spatial distribution which are important factors that significantly influence the change in mechanical properties of the FRC and the accurate measurement of porosity [12]. UT is also time consuming and limited to thin samples with flat surfaces. Additionally, the high anisotropy of FRCs results in more complex responses which are more difficult to analyse.

Like many scientific and engineering fields, recent developments in machine learning (ML) and more powerful compute hardware present an opportunity to develop data-driven defect detection and evaluation models [13][14][15]. There is strong justification to use ML for this specific problem type. Analytical models struggle to account for all the variables affecting the ultrasonic response of a porous FRC, and ML excels at finding complex non-linear relationships when provided with sufficient, high quality data. However, these datasets are not readily available or feasible to acquire in large quantities due to the limitations of current detection methods. One possible route for acquiring this data is to generate synthetic datasets.

This study investigates the application of ML to porosity detection in FRCs by generating large datasets of synthetic ultrasonic responses for a specific carbon-fibre reinforced polymer (CFRP) specimen. Section 3 describes the development of a 2D finite element (FE) simulation used to generate the datasets, Section 4 details the data generation program used to generate

large, diverse datasets, and Section 5 describes the selection and training of multiple ML models. Finally, The results from ML model testing are presented and discussed in Sections 6 and 7.

2. Ultrasonic testing background

Ultrasonic testing (UT) is a non-destructive inspection technique used to evaluate materials, components, and assemblies. By measuring the response of a part/specimen to an ultrasonic excitation, UT allows technicians to detect defects or irregularities within a part without destroying the part. A typical UT inspection setup consists of a transducer to transmit the ultrasonic wave, a receiver to measure the response, a couplant to ensure good coupling between the transducer and the specimen, and an oscilloscope to inspect response signals.

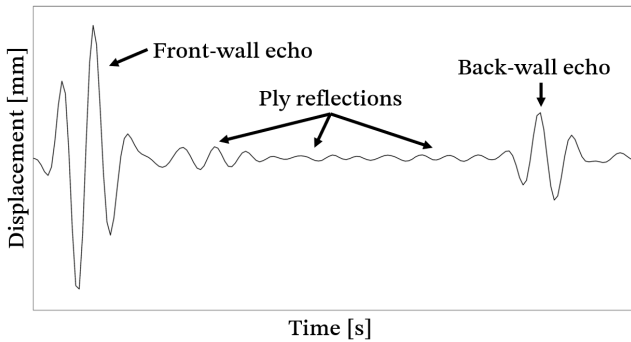


Figure 1. A typical time-displacement response for an ultrasonic response from an FRC. Key features of the response are labelled.

In this study, a pulse-echo UT inspection is simulated. This means the transducer and receiver are combined since the response is measured at the same location as the excitation. The response can be measured as a displacement or signal gain on an oscilloscope. In this simulation, the response is measured as a time-displacement signal, as shown in Fig. 1. Since the part under inspection is an FRC, the response will consist of a front-wall echo, intermediary reflections from the plies, and a back-wall echo which signifies the bottom surface of the specimen.

As mentioned in Section 1, signal attenuation is an important factor to consider when using UT to detect porosity. Attenuation is measured by analysing the reduction in amplitude of the back-wall echo relative to the front-wall echo while also accounting for beam divergence losses.

3. Finite element simulation

3.1. Dataset requirements and scope

The goal of the FE simulation is to produce large quantities of input data for ML model training, this input data being the ultrasonic response of a CFRP specimen with variable porosity. To produce reliable and insightful output from the ML model, it is paramount that the input data is high quality and sufficient quantity.

Data quantity. Sufficiently large datasets must be generated in a short time frame (2-3 weeks). Therefore, the simulations must run within the order of seconds (not minutes).

Data diversity. It is crucial that the training data has sufficient variability to ensure the ML model is robust and generalisable. By incorporating a wide range of input examples, the ML model can handle unseen scenarios more effectively and avoid overfitting. Overfitting occurs when a model learns specific details about the training data that do not generalise well to unseen data. Therefore, a diverse dataset helps the ML model extract and learn generalisable features, enhancing its ability to predict porosity accurately in real-world conditions.

Data accuracy. The datasets must be representative of real ultrasonic responses, otherwise, there is a risk that the ML model will make predictions based on signal features that are present in the simulation that are not present in real signals. To minimise the likelihood and impact of this occurring, the FE model is tested and validated thoroughly after each additional modelling stage and is finally compared against a known pristine signal (assumed to be from a specimen with no porosity) which was gathered experimentally in another study. The following sections describe the process of building the FE simulation to match the experimentally gathered signal.

The 2D FE model helps to achieve the *data quantity* goal as it is a small model which can be solved quickly while still capturing the complex acoustic behaviour of the CFRP. However, it is important to recognise that the FE method does not capture all of this complex behaviour, especially when reduced to 2D. The accuracy of the data generated will be limited by this.

3.2. Meshing and solver specification

The FE simulation is built using the BristolFE codebase [16] written in MATLAB [17]. BristolFE supports 2D plane-strain models built from a mesh of 3-node linear 2D plane-strain triangular elements (CPE3) for solids, 3-node linear 2D acoustic triangular elements (AC2D3) for fluids, and an interface element (ASI2D2) to couple solid and fluid layers [18]. A plane-strain model is used because it produces more accurate responses than plane-stress models. In this study, an isometric mesh is used to keep element sizes uniform which is important for ultrasonic FE simulations. This minimises the effect of numerical dispersion whereby high frequency wave components travel at different speeds to low frequency components.

To solve the time-domain response of the FE model from an ultrasonic excitation load, BristolFE solves the general system equation for node displacements using an explicit time-marching algorithm:

$$\mathbf{f}(t) = \mathbf{M}\ddot{\mathbf{u}}(t) + \mathbf{C}\dot{\mathbf{u}}(t) + \mathbf{K}\mathbf{u}(t) \quad (1)$$

Eq. 1 discretises time, t , into time-steps at which displacements, $\mathbf{u}(t)$, are calculated based on the applied force vector at that instant, $\mathbf{f}(t)$, and the global mass matrices which define the system. \mathbf{M} represents the global mass matrix, \mathbf{C} is the global damping matrix, and \mathbf{K} is the global stiffness matrix. $\dot{\mathbf{u}}(t)$ and $\ddot{\mathbf{u}}(t)$ are the nodal velocity and acceleration vectors respectively which are used to perform this calculation.

When using the explicit method, the time-step, δt , must be less than a critical value given by the Courant–Friedrichs–Lowy (CFL) condition, otherwise the simulation may become unstable [19]. Eq. 2 defines the CFL condition:

$$\delta t < \frac{L_{\min}}{c} \quad (2)$$

where L_{\min} is the size of the smallest element, and c is the maximum speed of longitudinal sound waves in the FE model.

The MATLAB code used to generate the ultrasonic response datasets is available as a fork of the BristolFE repository on GitHub [20].

3.3. Model description

3.3.1. CFRP specimen

The FRC modelled in this study is a 4 mm thick CFRP specimen manufactured from unidirectional (UD) IM7/8552 prepreg material [21] and stacked with layup $[[90_2/0_2]_S]$. This CFRP specimen is used because it is the same specimen that was inspected in the experimental data which will be used to validate the accuracy of the output of the FE simulation.

The specimen is modelled as layers of UD lamina (plies) stacked according to the $[[90_2/0_2]_S]$ layup (two 90° plies followed by two 0° plies, repeated until totalling 32 layers, symmetric about the centre of the specimen). Fig. 2 shows the model geometry used in the simulation.

The UD plies are modelled using transversely isotropic stiffness matrices and lumped mass matrices. A nominal laminate density of 1570 kg/m³ is used to model the CFRP material [21]. Eq. 3 defines the 6x6 compliance matrix, \mathbf{S} , for the 0° ply [22]:

$$\mathbf{S} = \begin{bmatrix} \frac{1}{E_t} & -\frac{v_t}{E_t} & -\frac{v_f}{E_f} & 0 & 0 & 0 \\ -\frac{v_t}{E_t} & \frac{1}{E_t} & -\frac{v_f}{E_f} & 0 & 0 & 0 \\ -\frac{v_f}{E_f} & -\frac{v_f}{E_f} & \frac{1}{E_f} & 0 & 0 & 0 \\ 0 & 0 & 0 & \frac{1}{2G_f} & 0 & 0 \\ 0 & 0 & 0 & 0 & \frac{1}{2G_f} & 0 \\ 0 & 0 & 0 & 0 & 0 & \frac{1+v_t}{E_t} \end{bmatrix} \quad (3)$$

This matrix is rotated 90° about the y -axis to obtain the 90° ply compliance matrix. These matrices are then inverted and reduced to 3x3 2D plane-strain stiffness matrices which are then used to assemble the element stiffness matrix, $\mathbf{K}^{(e)}$.

Transversely isotropic stiffness matrices reduce the number of required independent elastic constants from 21 to 5 using various symmetries. Values for these elastic constants are found through multiple sources to ensure the correct values are used in the simulation [23][24][25][26]. Table 1 provides the material properties used.

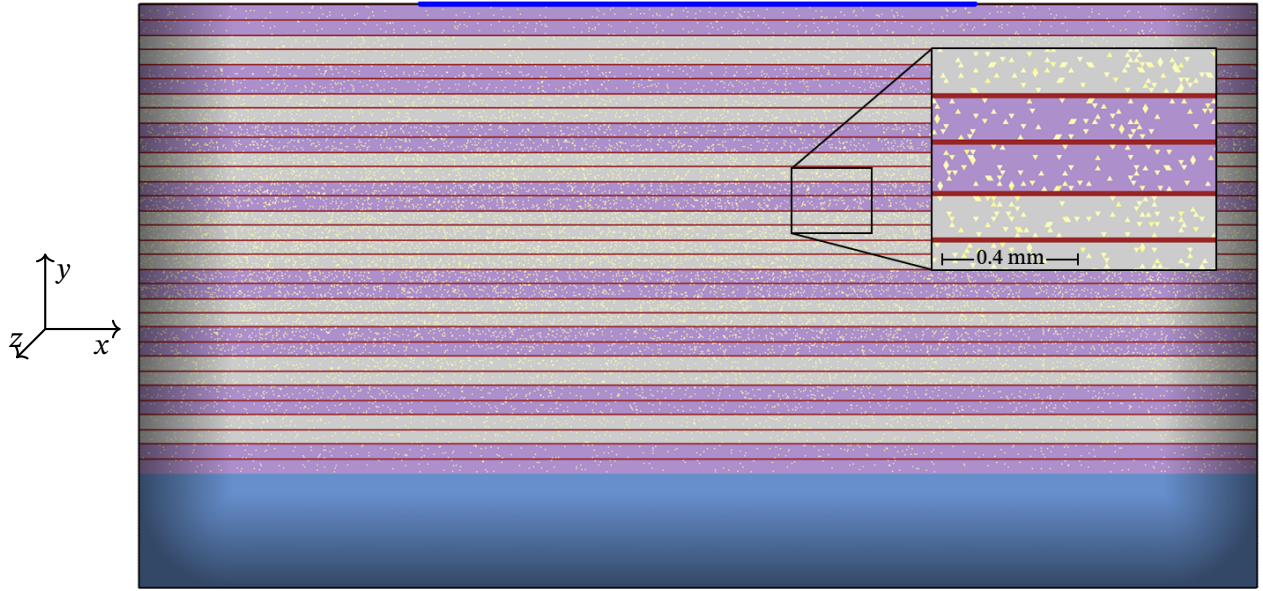


Figure 2. Geometry of CFRP model: 32 layers of UD IM7/8552 lamina, 4 mm thick, stacked in $[[90_2/0_2]_S]_S$ layup. The purple layers are the 90° plies, the grey layers are the 0° plies, and the dark red lines are the interlaminar resin layers. The atmosphere of small yellow elements represents pores. The thick blue layer on the bottom is a water boundary, and the dark blue line on the top surface is the transducer contact surface. The shaded region around the sides and bottom of the model indicate the absorbing boundary layer.

Table 1. Material properties used in FE simulation to model CFRP IM7/8552 UD lamina.

Property	Value	Unit
Young's Modulus (fibre), E_f	161.00	GPa
Young's Modulus (transverse), E_t	11.38	GPa
Poisson's Ratio (major), ν_f	0.320	-
Poisson's Ratio (minor), ν_t	0.436	-
Shear Modulus (fibre), G_f	5.17	GPa

Material damping is added to the CFRP model using the Rayleigh damping model. Eq. 4 defines the element damping matrix, \mathbf{C} , as a linear combination of the element mass and stiffness matrices, $\mathbf{M}^{(e)}$ and $\mathbf{K}^{(e)}$, respectively:

$$\mathbf{C}^{(e)} = \alpha \mathbf{M}^{(e)} + \beta \mathbf{K}^{(e)} \quad (4)$$

The mass and stiffness damping constants are defined as $\alpha = 0$ and $\beta = \frac{1}{2\pi f_c Q}$ where f_c is the centre frequency of the ultrasonic excitation, and Q is the quality factor. Delrue and Van Den Abeele modelled damping using this method [27] in a 3D ultrasonic FE simulation of a similar CFRP material and set $Q = 20$. In this study, $Q = 5000$ is required to obtain

reasonable damping behaviour from the simulation, otherwise damping is far too high and causes the signal to dissipate completely.

For simplicity, surface roughness and ply waviness are not modelled. Not modelling ply waviness is acceptable since the width of the model is small enough (<10 mm) for ply waviness to be negligible at that scale.

3.3.2. Boundaries

The experimental data was collected in water immersion. This means the specimen was inspected underwater. To simulate this, a water boundary is modelled at the bottom surface, however, a top water boundary is not modelled due to a known issue with BristolFE which causes instability at solid-fluid interfaces. Since the transducer is on the top surface, this instability contaminates the output very quickly. This can be alleviated by further decreasing the time-step, however, this significantly increases the simulation time without significantly changing the response.

An absorbing boundary is used to dissipate the energy of acoustic waves travelling into the edges of the model. This is done to avoid edge reflections which would not be seen in a real response. The absorbing boundary

is modelled using the damping power-law relation defined in Eq. 5:

$$\mathbf{C}^{(e)} = D_{\max}(\mathbf{M}^{(e)})^p \quad (5)$$

where the maximum damping coefficient, $D_{\max} = 3.1415 \times 10^{-7}$, and the exponent, $p = 3$, are set to the default values used by BristolFE.

3.3.3. Ultrasonic excitation load

The experimental data was gathered using a 128 element, linear, phased array ultrasonic transducer (PAUT) manufactured by Imasonic [28]. Fig. 3 shows the geometry of the contact surface of the PAUT with the specimen.

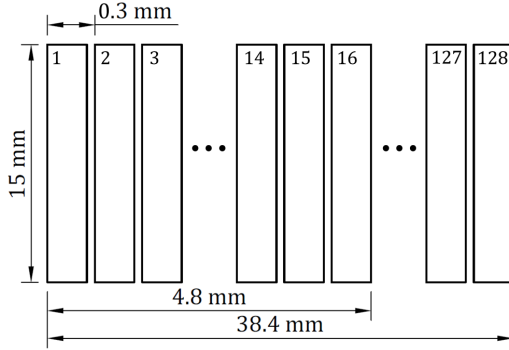


Figure 3. Geometry of PAUT linear array with numbered elements 1–128. Dimensions for 16 and 128 elements are shown.

To reduce the size of the FE model, only 16 of the 128 transducer elements are modelled. These 16 elements act analogously to using the full 128 array, except at a smaller scale. The ultrasonic excitation load is then applied to nodes at the top of the specimen. Since a pulse-echo inspection setup is used, displacements are recorded from the same location as the applied load.

The excitation signal used in the experimental setup was a Gaussian-modulated sinusoidal pulse. This signal is replicated in the FE simulation and is defined using Eq. 6:

$$s(t) = \exp \left[\left(\frac{2t f_c}{n} \right)^2 \ln(\beta) \right] \cdot \sin(2\pi f_c t) \quad (6)$$

where the signal, $s(t)$, is defined over a time, t , for a centre frequency, f_c , and a number of cycles, n . To

match the experimental setup, $f_c = 5$ MHz and $n = 3$ are used. The parameter β defines the point of -40 dB attenuation in the signal envelope and is set to 0.01.

It is assumed that there is perfect coupling between the transducer and the top surface of the specimen, and the transducer elements are in perfect condition. Therefore, the signal noise introduced from both of these factors is assumed to be negligible.

Note that displacements are normalised relative to the front-wall signal, so the figures presented in this study show no units on the displacement axes.

3.3.4. Interlaminar resin layers

In laminated composites, the thickness of the interlaminar resin layer is almost negligible compared to the thickness of the plies. However, when simulating the CFRP model without a resin layer, its ply reflections are very weak in the response profile. This does not correspond to real-world behaviour or what is seen in the experimental response.

The reason why the reflectivity of the plies is insufficient may be because the CFRP specimen is modelled as 2D. This results in the 0° ply losing its dominant (fibre-direction) stiffness component and being reduced to its transverse stiffness properties after the plain-stain constraint is applied. This may have an adverse effect on the reflectivity of the plies. It is also possible that the lack of surface roughness or ply waviness in the model could reduce the reflectivity of the plies.

To improve ply reflectivity, a relatively thick interlaminar resin layer is modelled. Fig. 4 shows the comparison between the CFRP response with a resin layer and without. Note that the 'With resin layer' response shifts to the right because the material properties of the resin cause the signal to slow down which causes slightly delayed reflections.

The reason this improves reflectivity can be explained by looking at the acoustic impedances of each material. Acoustic impedance is a material property that measures the resistance a material presents to a sound wave. It can be calculated using the speed of sound in a material, c , the density of a material, ρ , and its Young's Modulus, E . Since the speed of sound of a material can

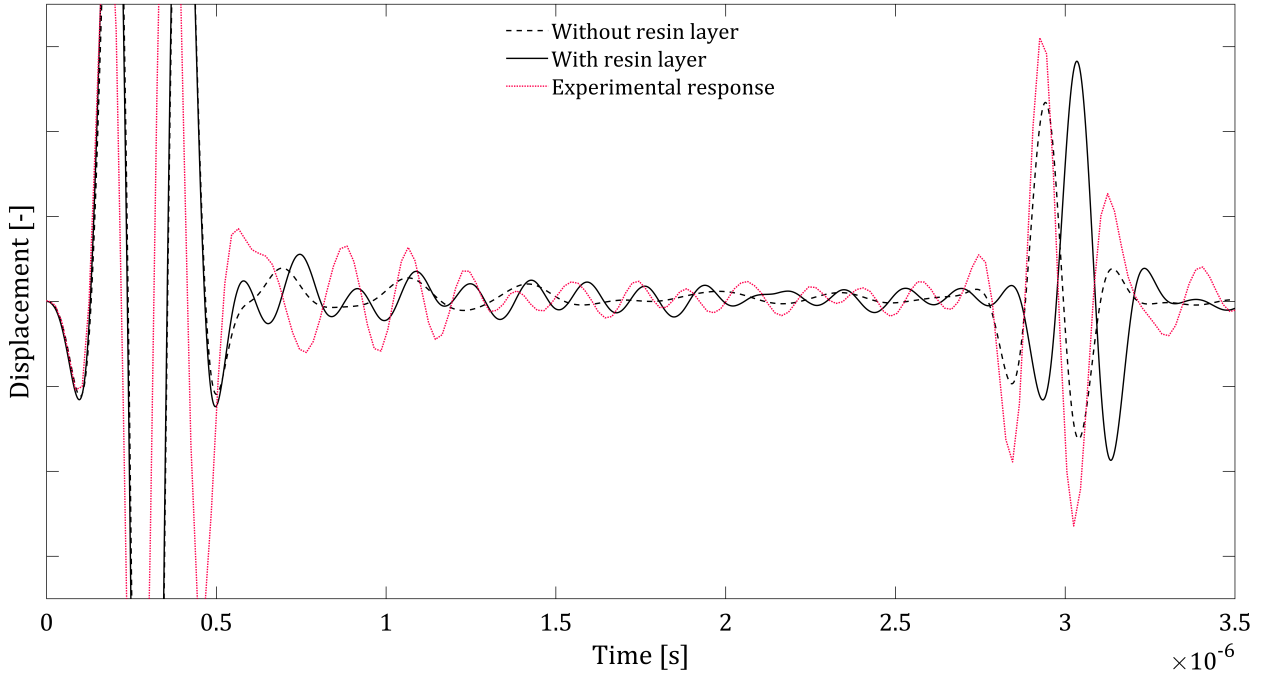


Figure 4. Plot comparing the experimental ultrasonic response to the simulated responses with and without interlaminar resin layers.

be approximated using $c = \sqrt{\frac{E}{\rho}}$, acoustic impedance, Z , can be approximated using Eq. 7:

$$Z = \rho c = \rho \sqrt{\frac{E}{\rho}} = \sqrt{E\rho} \quad (7)$$

This can then be used to describe the reflectivity of a material boundary by calculating the reflectivity coefficient, R , between one material with $Z = Z_1$ and another material with $Z = Z_2$. Eq. 8 shows how R is calculated:

$$R = \frac{Z_2 - Z_1}{Z_2 + Z_1} \quad (8)$$

Therefore, the reflectivity between the plies is increased by introducing a more significant change in acoustic impedance. Table 2 shows that the R value between the resin layer and the 90° ply is highest, in turn, increasing the reflectivity of the interlaminar boundary.

Table 3 shows the material properties used to model the resin layer [29]. The resin layer is then calibrated to

improve the accuracy of the simulated response with respect to the experimental response.

Table 2. Estimated reflectivity coefficients for different combinations of materials used in the FE model.

	Material 1	0° ply	Resin	Resin
Material 2	90° ply	90° ply	0° ply	
R	0.419	0.619	0.270	

Table 3. Material properties used in the simulation to model the interlaminar resin layer.

Property	Value	Unit
Young's Modulus	4.67	GPa
Poisson's Ratio	0.370	-

3.4. Model validation

To verify that the transversely isotropic stiffness matrices are working as intended, the wave speed is measured for both ply materials. It is expected that the 0° ply will have isotropic behaviour since its transverse properties are only present in the 2D model, and the 90° ply will have a wave speed in the x direction (horizontally), v_x , that is a multiple of its wave speed in the y direction, v_y . The transverse speed of sound in

Table 4. Speed of sound in each ply layer in the x direction (horizontally), v_x , and the y direction, v_y .

Material	v_y [m/s]	v_x [m/s]
90° ply	3070	10500
0° ply	3090	3170

CFRP should be approximately 3000 m/s [30]. Table 4 shows the results from these tests and shows that the stiffness matrix is working as intended.

Convergence testing proved to be more complicated than expected due to complex dependencies between the size of the elements used to construct the mesh, the resin layer, and the damping model. The resin layer is modelled to be 1 element thick, therefore, it scales with element size and its effect on the response becomes negligible at small element sizes. Furthermore, it was discovered that the damping model (defined in Eq. 4) has a complicated dependence on the size of the elements. Therefore, these features of the model are temporarily disabled to see if the model converges without them. Fig. 5 confirms that the model converges at around 15 elements per wavelength by showing the convergence of the back-wall echo (where convergence is most difficult). Literature supports this claim, citing 10–20 elements per wavelength as a recommended minimum resolution for ultrasonic FE simulations [31][32].

Finally, the simulated response is validated against the experimental response to see how accurately it represents a real response. This is shown in Fig. 6. This final response is obtained after numerous hours

of iterating and calibrating the model described in the previous sections.

Given the known limitations of the model — the lack of fibre-direction stiffness component for the 0° ply, poor ply reflectivity, lack of upper water boundary — the simulated response corresponds well to the profile of the experimental response. The main improvement that could be made is to match the phase and amplitude of the early ply reflections since they do not correspond well. This likely occurs due to the lack of top surface water boundary, meaning waves do not lose any energy when reflecting off the top surface of the specimen.

It is important to note that BristolFE has a limitation where it does not correctly calculate front-wall echos in this configuration of the FE simulation. Therefore, the front-wall echos are not considered during model validation. This limitation also means attenuation is difficult to measure — this is further discussion in the following section.

3.5. Porosity modelling

3.5.1. Background

Porosity in FRCs is characterised by the size, morphology, and distribution of the pores which make up this porosity. Pore size correlates with the level of porosity [33] and can be classified as micro-, meso-, and macro-pores. Generally, micro-pores are located within tows (between fibres), meso-pores are located between tows, and macro-pores are located in larger areas within the polymer matrix. Pore morphology can be spherical, cylindrical, flat, or irregular.

The characterisation of porosity is not very well generalised across different FRCs in the literature. This is due to its dependence on a wide range of factors such as manufacturing process, reinforcement structure, stacking sequence, and prepreg conditions [2]. Therefore, the porosity model used in this study focuses on replicating the effect of porosity on the ultrasonic response rather than accurately modelling the pores themselves. This means that pore size, morphology, and location within the CFRP model is not always realistic, but intends to produce accurate response data — which is ultimately what is required for the ML model.

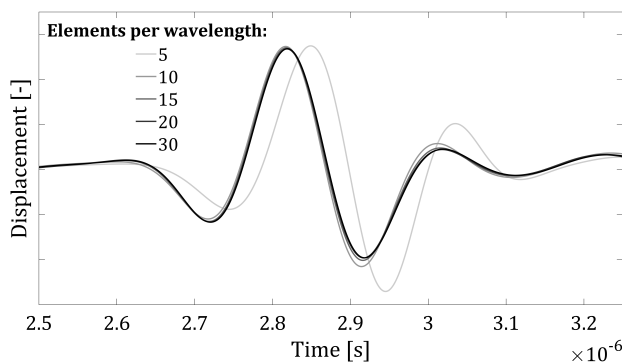


Figure 5. Plot of five simulated responses with varying elements per wavelength to test convergence. Zoomed into the back-wall echo because it is most difficult to converge.

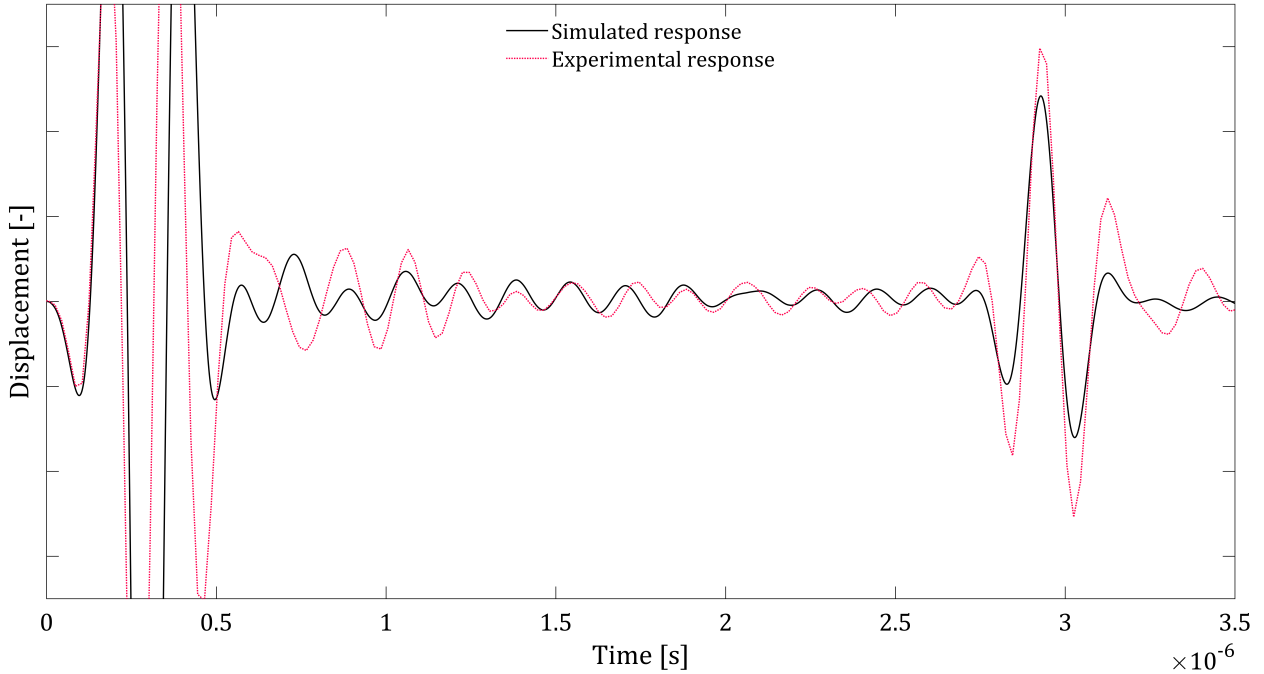


Figure 6. Plot of the simulated response over the experimental response. Good correspondence verifies the accuracy of the simulated response.

The effect of porosity on the ultrasonic response of UD CFRPs was investigated by Stone and Clarke [6]. They found a bi-linear relationship between porosity, p_v , and attenuation coefficients, α , for ultrasonic responses. Up to $p_v = 1.5\%$ this relationship is linear. Therefore, to create a realistic porosity model, the porosity model is calibrated to reproduce this linear relationship between α and p_v . Eq. 9 approximately defines this linear relationship found by Stone and Clarke:

$$\alpha \approx 0.833p_v + 0.5 \quad (9)$$

However, due to limitations in how BristolFE calculates front-wall echo amplitudes, measuring α accurately is difficult. Furthermore, instability in the simulation means α cannot be measured using the double distance method so losses due to beam divergence cannot be accounted for [34]. Therefore, the porosity model is calibrated to simply have a linear relationship between α and p_v rather than matching the gradient and y-intercept of the relationship exactly. So that higher porosity levels can be included in the final datasets, it is assumed that the linear relationship holds up to $p_v = 3\%$.

To approximate the attenuation coefficient, α , from only one back-wall echo, Eq. 10 is used:

$$\alpha \approx \frac{20 \log \left(\frac{1}{\hat{Y}_{\text{back}}} \right)}{2t} \quad (10)$$

where \hat{Y}_{back} is the normalised maximum amplitude of the back-wall echo and t is the specimen thickness.

3.5.2. Pore damping model

By modelling porosity as an increase in damping in the FE model, the pores can be calibrated to produce the linear $\alpha-p_v$ relationship. To model this increase in damping, a specific number of elements required to achieve a level of porosity, p_v , are reassigned their damping coefficients, β , for higher damping coefficients, β_{pore} . Eq. 11 defines this reassignment:

$$\beta_{\text{pore}} = C\beta A_{\text{pore}} = C\beta \left(1 - \pi\sqrt{3} \frac{r_{\text{pore}}^2}{H^2} \right) \quad (11)$$

where C is the calibration factor used to tune the amount of damping of the pores, and A_{pore} is the factor used to scale the damping with the size of the pore which is based on removing a circular pore of radius, r_{pore} , from a triangular element of height, H .

This method allows the damping of the pores to be scaled in proportion to r_{pore} , and r_{pore} can be smaller than H (if pores are modelled by removing elements, they would be restricted to the height of the elements, H). p_v can also be carefully controlled using the same A_{pore} factor to reduce the density of the elements in proportion to the size of the pore assigned to them.

3.5.3. Pore distribution

The pores are distributed uniformly along the x -axis of the model, and distributed via a truncated normal distribution along the y -axis of the model. By varying the mean and variance of this normal distribution, the depth and uniformity of the porosity distribution can be controlled. In Section 3.3.1, Fig. 2 shows what the CFRP model looks like with 1% porosity distributed centrally in the specimen.

3.5.4. Pore characterisation and calibration

In summary, the pores modelled in this FE model are characterised as cylindrical, intralamina, micro-pores between 1–5 μm radii, normally distributed along the y -axis and uniform in x . The porosity model also produces the required linear relationship between α and p_v . This is shown in Fig. 7 where 50 simulated responses with random p_v are plotted against α . The linear best-fit line for α - p_v is defined in Eq. 12:

$$\alpha \approx 0.140 p_v + 1.936 \quad (12)$$

Furthermore, α increases with excitation frequency in the simulation which corresponds to what was found by Stone and Clarke in their work — further validating the damping model method. However, it should be noted that the attenuation coefficient for 0% porosity is high in the simulation. This is discussed as a potential source of error in Section 7.

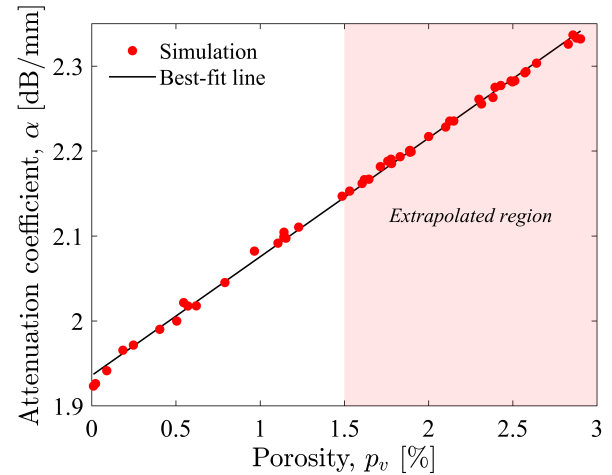


Figure 7. Plot of α against p_v showing a linear relationship and the extrapolated region where the linear model would normally change to a steeper gradient.

4. Data generation method

This section defines the process of generating datasets of the required *quantity*, and *diversity* for input into the ML model. Data quantity was addressed throughout the development of the FE simulation where multiple decisions were made to optimise and prioritise the runtime of the FE simulation. The final simulation takes <30 seconds to complete which is sufficient to generate tens of thousands of training examples within a few weeks (when running two simultaneous data generation scripts on a Dell XPS laptop).

Data diversity is achieved by running the FE simulation with variable input parameters. This is done by randomly sampling parameter values from normal distributions defined by their default values. For instance, the specimen thickness, t , is randomly sampled from a normal probability distribution, $N(t_0, (0.01t_0)^2)$, where $t_0 = 4$ mm is its default value, and the standard deviation is defined as a percentage of t_0 . This means 68% of randomly selected values for t will be within 1% of t_0 . This is replicated for all simulation parameters that are varied. Some parameters are given larger variances than others (1–10% of their default values) to reflect more realistic variances for those parameters.

Porosity-related parameters are not varied with normal distributions and instead vary over uniform distributions. This ensures the full range of porosity conditions are equally available to the ML model for training.

Table 5 provides the specification for the FE simulation, including the default values used for each parameter and which parameters are varied using the technique described.

Table 5. Simulation specification used to generate porosity response datasets. Value column indicating the default value or a range. Varied column indicating if a parameter is manually varied (Y), or is not (N).

Parameter	Value	Unit	Varied
Simulation time	3.5	μs	N
Elements per wavelength	15	-	N
Element height	13.2	μm	N
Specimen thickness	4.0	mm	Y
Model height	5.0	mm	N
Model width	9.6	mm	N
Ply density	1570	kg/m^3	Y
Ply stiffness components (Table 1)	-		Y
Ply damping quality factor	5000	-	Y
Resin density	1301	kg/m^3	Y
Resin Young's Modulus	4.67	GPa	Y
Water density	1000	kg/m^3	Y
Water bulk modulus	3.38	GPa	Y
Porosity range	[0 3]	%	N
Pore radius range	[1 5]	μm	N
Pore radius mean	$\pm 3^1$	μm	N
Pore radius variance	1	μm^2	Y
Pore distribution mean	2	mm	Y
Pore distribution variance	1	mm^2	Y

Using the data generation process described, 31,462 responses are generated. Four additional smaller datasets are then sampled from this dataset so that the performance of the ML model can be measured for smaller dataset sizes. Additionally, a sixth dataset is created which has less variability in simulation parameters. Finally, all responses are resampled to match the sampling frequency used to collect the experimental data (50 MHz).

The completion of the data generation component marks the end of the work done in MATLAB, where over 2000 lines of code were added to the custom BristolFE codebase.

¹Scales with level of porosity

5. Machine learning model training and testing

The porosity response datasets contain time-series responses with porosity labels. Therefore, this problem requires a regression ML model that attempts to find features/predictors in the responses that allow it to predict porosity in the CFRP model accurately. This is a supervised technique which means the model is trained on labelled datasets where the correct outputs (the porosity values) are known.

Deep learning (DL) is a subset of ML which focuses on the use of artificial neural networks with ‘deep’ interconnected layers of neurons (as opposed to ‘shallow’ ML models). This greatly increases the complexity of the model but offers the benefit of automatic feature extraction. This means that features in the responses (such as signal energy or frequency-dependent features) do not need to be manually selected or evaluated, instead, the DL model is given raw time-series data and determines which features to use without human intervention [13]. Additionally, by evaluating which datapoints the DL model is using in the response to make predictions, the ‘importance’ of each datapoint/feature can be calculated and visualised. Therefore, using DL models is advantageous in this study to speed up and automate feature extraction and analyse the importance of different parts of the response for making porosity predictions.

ML model development historically includes several stages of development, each requiring extensive background knowledge and experience in ML in order to achieve state-of-the-art performance. Automated ML (AutoML) was developed to simplify and speed up this process of model development for non-experts without compromising on the performance of the model. AutoGluon is an open-source AutoML Python library [35] suitable for the ML model development in this study. The AutoGluon-Tabular API allows developers to input unprocessed structured datasets (such as CSVs of signal data) for regression and classification tasks with a focus on combining multiple ML/DL models to optimise prediction accuracy. These are called ensemble models.

To train the AutoGluon ML models, each of the six datasets are input into the AutoGluon-Tabular API to train six different ML models. Each ML model is

trained and tested on 80% and 20% of its corresponding dataset respectively. An optimal model is selected using the root-mean-squared error (RMSE) performance metric.

To test the ML models, four key questions are investigated in the following section:

1. How accurate are the ML models relative to existing methods (better than $\pm 0.5\%$ porosity)?
2. How do the ML models perform on real-world data?
3. How does performance scale with dataset size?
4. Do the ML models rely on attenuation to predict porosity? I.e., how do the ML models perform relative to the linear Stone and Clarke model?

6. Results

AutoGluon is given five datasets containing 3584, 6374, 12354, 25793, and 31803 examples from the same population of responses, and one dataset of 3584 examples from another population with less variability. The trained ML models are labelled Model 1–6 respectively. Using RMSE as the performance metric, the weighted ensemble model [36] performs the best on all six datasets. However, the CatBoost model [37] has similar performance (RMSE = 0.144% porosity) and has an inference time that is 1000 times faster at ~ 0.1 ms. The weighted ensemble model actually contains the CatBoost model in its ensemble architecture, but because it also contains many other models, it has a significantly longer inference time.

The performance of the weighted ensemble models is evaluated using their respective test sets and 56 experimentally gathered responses. The experimental responses are assumed to come from a pristine composite, so 0% porosity is assumed. The RMSE for each model on both datasets is summarised in Table 6.

Table 6 shows that the models perform well on both datasets. However, RMSE increases with dataset size for the experimental responses. Furthermore, Model 6 has a lower RMSE than Model 5 for both datasets despite having 10 times less data. To analyse this further, Fig. 8 is plotted to show how the proportion of predictions made by each model varies with increasing error tolerance. This effectively measures the accuracy of the models.

Table 6. Performance of weighted ensemble models on 80% of their corresponding dataset (*contains data with reduced variability). RMSE shows model performance on 20% of its dataset (the test set). RMSE (exp) shows performance on 56 experimental responses.

Model ID	Dataset size	RMSE	RMSE (exp)
1	3584	0.247	0.092
2	6374	0.218	0.176
3	12354	0.179	0.177
4	25793	0.144	0.353
5	31803	0.132	0.307
6	3584*	0.113	0.239

Fig. 8 shows that Models 1–5 become more accurate as the number of training examples increases, and are able to make more predictions within tighter error tolerances. It also shows that Model 6 is less accurate than Models 1–5 at tighter error tolerances, but overall achieves more accurate predictions according to its lower RMSE.

To benchmark the ML models against conventional methods, Model 5 is tested against the attenuation-porosity relationship found by Stone and Clarke, as described in Section 3.5.4. Using Eq. 12 and 9, porosity is recovered from attenuation coefficients for the simulated and experimental data respectively. Fig. 9 shows the performance of each model on the simulated data, and Fig. 10 shows the performance of each model on the 56 experimental responses. This is plotted separately because all experimental data is assumed to have 0% true porosity, so it would appear as a vertical line on Fig. 9. Fig. 9 suggests that Model 5 performs better than the linear model as predictions lie closer to the ‘perfect predictions’ line. This is also true for the experimental data as predictions lie closer to 0% porosity.

To investigate how each ML model is making predictions, the importance of each part of the response is calculated. This is called ‘feature importance’. This is done by calculating how much each feature/time-step on the response contributes to the final prediction. Fig. 11 plots the importance of each time-step for each model. An arbitrary response is plotted as a reference point, so the columns may not be perfectly aligned. An importance of 1.0 indicates that an ML model considers that feature ‘the most important’, and darker columns indicate that multiple ML models use that same feature.

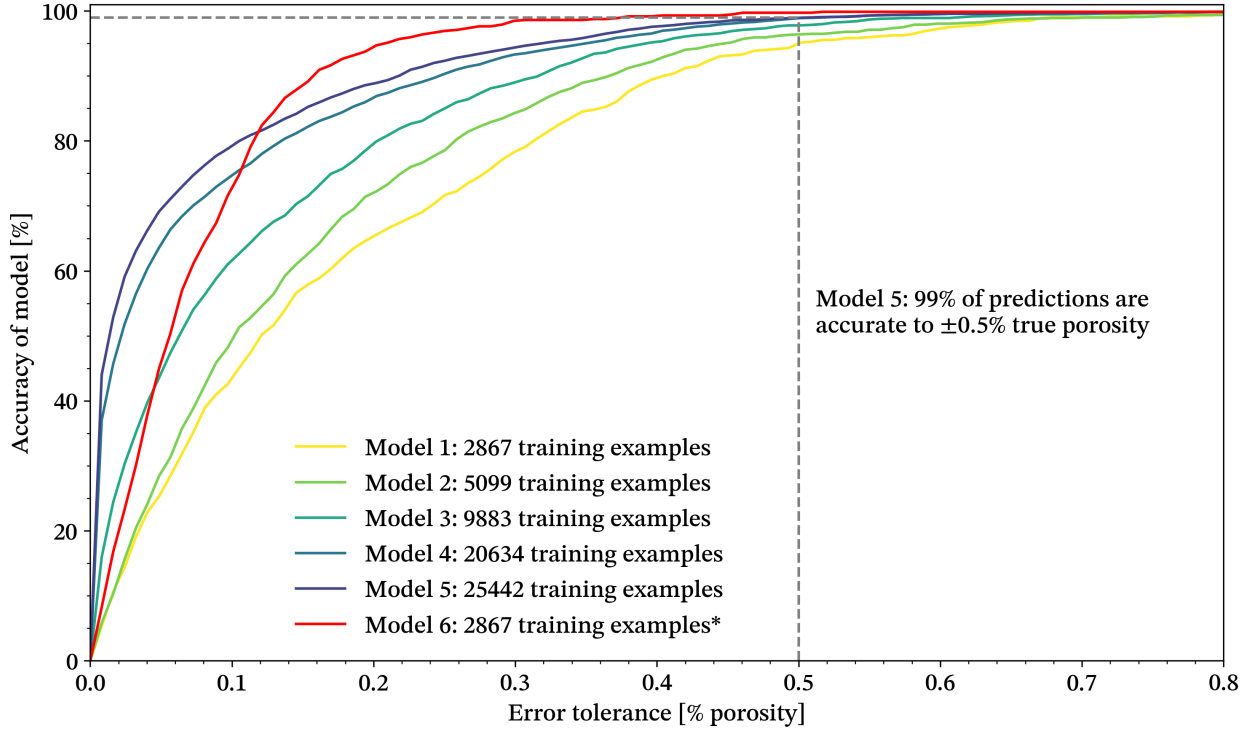


Figure 8. Plot showing the proportion of predictions made by each ML model within increasing error tolerances (*contains data with reduced variability).

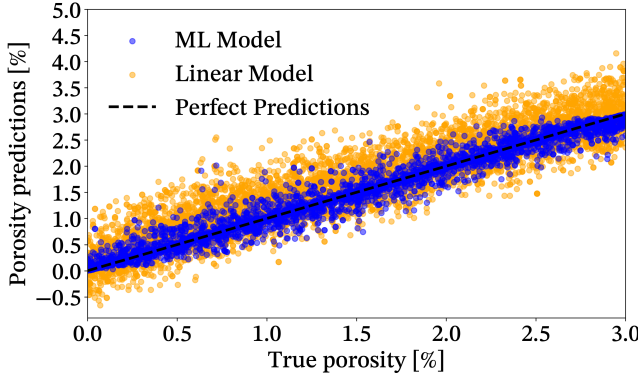


Figure 9. Porosity predictions vs true porosity using Model 5 on its test set and the linear model on the same dataset.

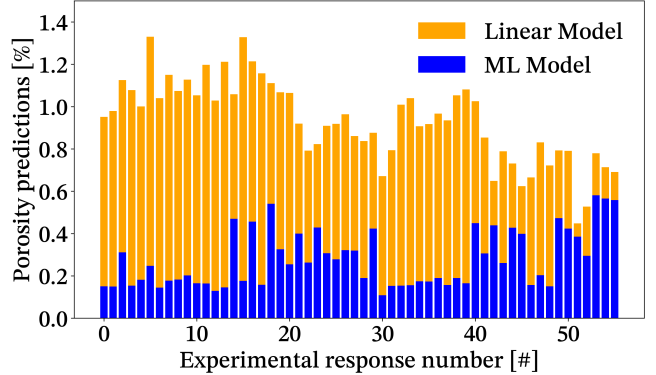


Figure 10. Porosity predictions using Model 5 and the linear model on 56 experimental responses.

Fig. 11 suggests that Models 1–5 almost solely rely on features in the back-wall echo to make accurate predictions. This corresponds to how attenuation is calculated, therefore, it is likely that the models are using attenuation to make predictions. Model 6 also prioritises the back-wall echo but relies more on features in the ply reflections than the other models.

7. Discussion

Fig. 8 shows that the ML models can meet the $\pm 0.5\%$ porosity error tolerance target at a high accuracy of 99%. This accuracy may be further improved with more data since there is no evidence that the accuracy curve has reached an asymptote. Therefore, the ML models perform similarly to the established porosity detection methods outlined in Section 1 on synthetic data. However, it is more valuable to assess how the models

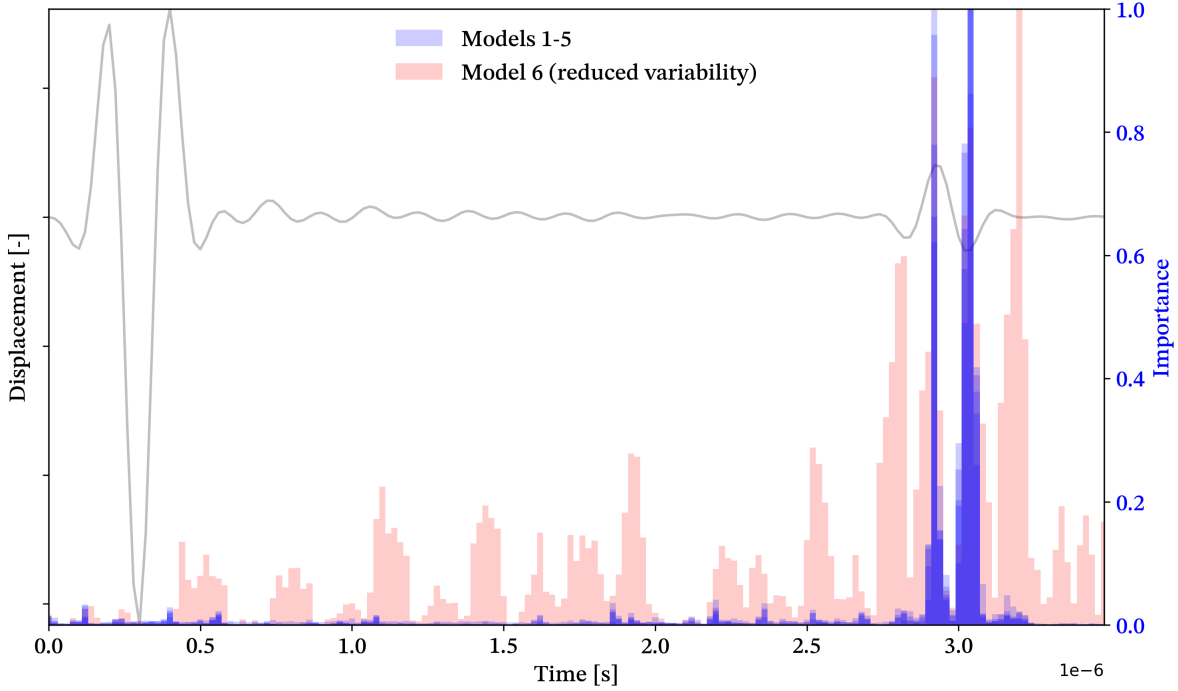


Figure 11. Feature importance plot showing how much each feature/time-step on the response contributes to the final prediction for Models 1–5 and Model 6 separately.

perform on real-world data. The pristine experimental data attempts to test this, however, it is difficult to come to any firm conclusions on the real-world performance of the models since the experimental dataset is limited in size and diversity. The true level of porosity is also unknown and is conservatively assumed to be 0%. That being said, Table 6 and Fig. 10 indicate that the ML models perform well on data they have not seen before and perform significantly better than the linear model on the same data.

Fig. 11 indicates that the models are likely using attenuation to make predictions due to the high importance attributed to the back-wall echo. However, other features in the echo may also be calculated such as frequency content, shape, or phase velocity. It is also possible that some features of the ply reflections are still contributing to prediction accuracy despite the low importance attributed to this part of the response. The models consistently perform better than the linear model on synthetic and experimental datasets so it is unlikely that the models rely on a trivial calculation to make predictions. Overall, the results suggest that the ML models may be able to reveal new methods of calculating porosity from ultrasonic responses that conventional techniques do not exploit, however, fur-

ther testing will be necessary to determine how these models achieve this and if a more simple, non-ML-based method could achieve similar results. That being said, it is very difficult to determine which of these 'higher-level' features are being calculated from the response due to the complexity of the weighted ensemble model. Furthermore, the ML models may not be performing much better than the linear model if attenuation coefficients were not calculated accurately during data generation. Section 3.5.4 details why this is likely.

Model 6 achieves significantly better accuracy than Model 1 after being trained on the same size dataset but with less variability. This behaviour may be the result of overfitting. With reduced variability in the data, it is likely that Model 6 learned to predict more accurately using less training examples, in turn, the model uses features in the responses that are highly specific to the simulated CFRP specimen and do not generalise well to real-world responses. This may explain why, in Fig. 11, Model 6 uses different features compared to the other models. Model 6 performs well on the experimental data, but since this data is limited, further testing is necessary to conclude that Model 6 is overfitting.

Based on the good performance of the ML models on both synthetic and real-world data, the data generation method has proven to be effective within the scope of this study. The 2D FE model is simple enough to generate responses quickly, but accurate enough to allow the ML models to make accurate predictions on the experimental data. Modelling the effect of porosity rather than the pores themselves means larger elements can be used in the FE model which greatly reduces simulation time. However, further testing is required to validate the porosity model against a wider range of real-world data, and to verify if this porosity modelling technique is applicable to different porosity conditions and pores of different sizes and morphology.

A potential industrial embodiment of this technology could consist of:

1. Configuring a simple 2D FE simulation for a specific FRC under inspection
2. Generating large datasets of responses
3. Training an optimal ML model to predict porosity based on these datasets
4. Loading the trained ML model onto UT hardware.

Using an ML with low inference time, such as the CatBoost model, would provide technicians with 1000's of porosity measurements per second — reducing the chance of anomalies and increasing confidence in the ML model output.

8. Conclusions & Recommendations

It has been shown that machine learning (ML) models are able to detect and quantify simulated porosity in carbon-fibre reinforced polymer (CFRP) using synthetic ultrasonic testing (UT) datasets. The accuracy of one of the ML models reaching 99% within an error tolerance of $\pm 0.5\%$ porosity on synthetic data which meets the standard of some existing porosity detection methods [6][10]. Similar performance is achieved on experimentally gathered responses, however, this dataset is limited and further testing is required to understand the performance of the models on real-world data. A framework is provided for how the detection method could be implemented in an industrial setting. Further investigations may consider this framework when defining design requirements for potential future embodiments of the technology.

Overall, the good performance of the ML models suggests that a simple 2D finite element (FE) model is able to produce the required UT datasets in sufficient quantity, quality, and diversity. However, there are key areas of the FE model which could be further developed to improve the accuracy of the output. Current limitations to the BristolFE finite element code [16] means front-wall echos are not calculated correctly, and there is instability when modelling solid-fluid boundaries. Without these limitations, attenuation can be calculated more accurately and UT inspections in immersion can be more accurately modelled.

The porosity modelling technique has shown to be effective within the scope of this study. However, further investigation is required to verify if this technique is applicable to different porosity conditions and pores of different sizes and morphology. Notably, the method of modelling the effect of porosity on the ultrasonic response instead of modelling the pores themselves presents a promising avenue for generating large datasets of ultrasonic responses for porous fibre-reinforced composites (FRCs).

It is still uncertain if the use of ML is essential to obtain these results and if simpler signal processing techniques can be used more effectively with less computational overhead. The models are shown to be predominantly relying on features in the back-wall echo to make predictions which corresponds to attenuation-based techniques [6]. There is also evidence that the models are performing non-trivial calculations that are not exploited by conventional methods. Further investigations should evaluate a wider range of conventional porosity detection techniques alongside ML models. The automated ML (AutoML) library used in this study, AutoGluon, relies on complex deep learning (DL) models, therefore, testing simpler ML models using different AutoML libraries, or bespoke ML models, should be investigated. Testing on data with greater and reduced variability should also be conducted since this study finds significantly different results for datasets with reduced variability. Finally, the ML models may perform better if they are given sets of multiple responses from the same location, rather than a single response per location. This would increase the information available to the ML model, and is already a common practice in industry through the use of phased array ultrasonic transducers (PAUTs).

References

- [1] R. Soni, R. Verma, R. Kumar Garg, and V. Sharma, "A critical review of recent advances in the aerospace materials," *Materials Today: Proceedings*, Aug. 12, 2023.
- [2] M. Mehdikhani, L. Gorbatikh, I. Verpoest, and S. V. Lomov, "Voids in fiber-reinforced polymer composites: A review on their formation, characteristics, and effects on mechanical performance," *Journal of Composite Materials*, vol. 53, no. 12, pp. 1579–1669, May 1, 2019.
- [3] N. C. W. Judd and W. W. Wright, "Voids and their effects on mechanical-properties of composites – an appraisal," *Sampe J*, vol. 14, pp. 10–14, 1978.
- [4] D. J. Hagemaire, "Nondestructive testing of advanced composites," *Materials Evaluation*, vol. 37, no. 7, pp. 43–49, 1979.
- [5] D. Purslow, "On the optical assessment of the void content in composite materials," *Composites*, vol. 15, no. 3, pp. 207–210, Jul. 1, 1984.
- [6] D. E. W. Stone and B. Clarke, "Ultrasonic attenuation as a measure of void content in carbon-fibre reinforced plastics," *Non-Destructive Testing*, vol. 8, no. 3, pp. 137–145, Jun. 1, 1975.
- [7] T. S. Jones, D. Polansky, and H. Berger, "Radiation inspection methods for composites," *NDT International*, vol. 21, no. 4, pp. 277–282, Aug. 1, 1988.
- [8] C. Muralidhar and N. K. Arya, "Evaluation of defects in axisymmetric composite structures by thermography," *NDT & E International*, vol. 26, no. 4, pp. 189–193, Aug. 1, 1993.
- [9] J. S. U. Schell, M. Deleglise, C. Binetruy, P. Krawczak, and P. Ermanni, "Numerical prediction and experimental characterisation of meso-scale-voids in liquid composite moulding," *Composites Part A: Applied Science and Manufacturing*, vol. 38, no. 12, pp. 2460–2470, Dec. 1, 2007.
- [10] G. Rao, B. Plank, and J. Kastner, "Comparison of different segmentation methods for porosity evaluation in CFRP-reference samples and comparison with real porosity samples," *e-Journal of Nondestructive Testing*, vol. 21, no. 2, Feb. 1, 2016.
- [11] E. A. Birt and R. A. Smith, "A review of NDE methods for porosity measurement in fibre-reinforced polymer composites," *Insight - Non-Destructive Testing and Condition Monitoring*, vol. 46, no. 11, pp. 681–686, Nov. 1, 2004.
- [12] H. Jeong and D. K. Hsu, "Experimental analysis of porosity-induced ultrasonic attenuation and velocity change in carbon composites," *Ultrasonics*, vol. 33, no. 3, pp. 195–203, May 1, 1995.
- [13] Y. Duan, T. Shao, Y. Tao, et al., "Automatic air-coupled ultrasound detection of impact damages in fiber-reinforced composites based on one-dimension deep learning models," *Journal of Nondestructive Evaluation*, vol. 42, no. 3, p. 79, Aug. 29, 2023.
- [14] S. Sambath, P. Nagaraj, and N. Selvakumar, "Automatic defect classification in ultrasonic NDT using artificial intelligence," *Journal of Nondestructive Evaluation*, vol. 30, no. 1, pp. 20–28, Mar. 1, 2011.
- [15] E. F. Simas Filho, Y. N. Souza, J. L. S. Lopes, C. T. T. Farias, and M. C. S. Albuquerque, "Decision support system for ultrasound inspection of fiber metal laminates using statistical signal processing and neural networks," *Ultrasonics*, vol. 53, no. 6, pp. 1104–1111, Aug. 1, 2013.
- [16] P. Wilcox, *Ndtatbristol/BristolFE-v2*, version cd69101, Ultrasonics and Non-destructive Testing Group, Jan. 25, 2024. [Online]. Available: <https://github.com/ndtatbristol/BristolFE-v2> (visited on 04/12/2024).
- [17] The MathWorks Inc, *MATLAB*, version 23.2.0.2428915 (R2023b), 2024.
- [18] Dassault Systèmes, *ABAQUS analysis user's manual*, version 6.6, 2009.
- [19] R. Courant, K. Friedrichs, and H. Lewy, "Über die partiellen Differenzengleichungen der mathematischen Physik," *Mathematische Annalen*, vol. 100, no. 1, pp. 32–74, Dec. 1, 1928.
- [20] D. Peppe, *Danielpeppe/BristolFE-v2*, version 79c64de, Feb. 14, 2024. [Online]. Available: <https://github.com/danielpeppe/BristolFE-v2> (visited on 04/12/2024).
- [21] Hexcel Corporation, "HexPly 8552 epoxy matrix," Hexcel Corporation, Product Data Sheet, 2023. [Online]. Available: [https://www.hexcel.com/user-area/content_media/raw/HexPly_8552_eu_DataSheet\(1\).pdf](https://www.hexcel.com/user-area/content_media/raw/HexPly_8552_eu_DataSheet(1).pdf) (visited on 04/13/2024).

- [22] eFunda, Inc. "Hooke's law for transversely isotropic materials." (2024), [Online]. Available: https://www.efunda.com/formulae/solid_mechanics/mat_mechanics/hooke_iso_transverse.cfm (visited on 05/06/2024).
- [23] N. Griya, K. C. Nithin Kumar, D. Pratap Singh, and A. Shaikh, "Finite element analysis of UD carbon-epoxy laminate under in-plane load," *Materials Today: Proceedings*, 10th International Conference of Materials Processing and Characterization, vol. 26, pp. 756–759, Jan. 1, 2020.
- [24] W.-G. Jiang, S. R. Hallett, B. G. Green, and M. R. Wisnom, "A concise interface constitutive law for analysis of delamination and splitting in composite materials and its application to scaled notched tensile specimens," *International Journal for Numerical Methods in Engineering*, vol. 69, no. 9, pp. 1982–1995, 2007.
- [25] K. Marlett, "Hexcel 8552 IM7 unidirectional prepreg: Qualification material property data report," National Institute for Aviation Research, Wichita State University, Wichita, KS, CAM-RP-2009-015 Rev A, Apr. 2011, pp. 33–34. [Online]. Available: https://www.wichita.edu/industry_and_defense/NIAR/Research/hexcel-8552/IM7-Unitape-2.pdf (visited on 04/13/2024).
- [26] T. K. O'Brien and R. Krueger, "Analysis of ninety degree flexure tests for characterization of composite transverse tensile strength," NASA Langley Research Center, Hampton, Virginia, NASA/TM 2001-211227, Oct. 2001. [Online]. Available: <https://dl.acm.org/doi/pdf/10.5555/888346> (visited on 04/13/2024).
- [27] S. Delrue and K. Van Den Abeele, "Three-dimensional finite element simulation of closed delaminations in composite materials," *Ultrasonics*, vol. 52, no. 2, pp. 315–324, Feb. 1, 2012.
- [28] IMASONIC SAS. "General purpose linear arrays," IMASONIC NDT. (2024), [Online]. Available: <https://www.imasonic.com/industry/general-purpose-arrays/> (visited on 04/16/2024).
- [29] R. Krueger, J. G. Ratcliffe, and P. J. Minguet, "Panel stiffener debonding analysis using a shell/3d modeling technique," *Composites Science and Technology*, The Sixteenth International Conference on Composite Materials with Regular Papers, vol. 69, no. 14, pp. 2352–2362, Nov. 1, 2009.
- [30] S. Bayat, A. Jamzad, N. Zobeiry, A. Poursartip, P. Mousavi, and P. Abolmaesumi, "Temporal enhanced ultrasound: A new method for detection of porosity defects in composites," *Composites Part A: Applied Science and Manufacturing*, vol. 164, p. 107259, Jan. 1, 2023.
- [31] F. Moser, L. J. Jacobs, and J. Qu, "Modeling elastic wave propagation in waveguides with the finite element method," *NDT & E International*, vol. 32, no. 4, pp. 225–234, Jun. 1, 1999.
- [32] E. Rosenkrantz, A. Bottero, D. Komatitsch, and V. Monteiller, "A flexible numerical approach for non-destructive ultrasonic testing based on a time-domain spectral-element method: Ultrasonic modeling of lamb waves in immersed defective structures and of bulk waves in damaged anisotropic materials," *NDT & E International*, vol. 101, pp. 72–86, Jan. 1, 2019.
- [33] K. I. Tserpes, A. G. Stamopoulos, and S. G. Pantelakis, "A numerical methodology for simulating the mechanical behavior of CFRP laminates containing pores using x-ray computed tomography data," *Composites Part B: Engineering*, vol. 102, pp. 122–133, Oct. 1, 2016.
- [34] B. Zoofan, "Measuring the attenuation coefficient of ultrasonic beams in materials," Jul. 1, 2017. [Online]. Available: <https://www.semanticscholar.org/paper/Measuring-the-Attenuation-Coefficient-of-Ultrasonic-Zoofan/d0a1f8ef29a42186bb3692803b6b64a905bc39b3> (visited on 04/19/2024).
- [35] N. Erickson, J. Mueller, A. Shirkov, et al., "AutoGluon-tabular: Robust and accurate AutoML for structured data," *arXiv preprint arXiv:2003.06505*, 2020.
- [36] R. Caruana, A. Niculescu-Mizil, G. Crew, and A. Ksikes, "Ensemble selection from libraries of models," in *Twenty-first international conference on Machine learning - ICML '04*, Banff, Alberta, Canada: ACM Press, 2004, p. 18. [Online]. Available: <http://portal.acm.org/citation.cfm?doid=1015330.1015432> (visited on 04/22/2024).
- [37] A. V. Dorogush, V. Ershov, and A. Gulin, "CatBoost: Gradient boosting with categorical features support," *arXiv preprint arXiv:1810.11363*, 2018.